Effects of Sulfide on the Corrosion Behaviour of 2205 Duplex Stainless Steels in HCl Solution

Xi Yang[1], Junlei Tang[1], Bernard Normand[2]

[1] *Southwest Petroleum University, Chengdu, China PR, tangjunlei@126.com*
[2] *Université de Lyon, INSA Lyon, MATEIS UMR CNRS 5510, Lyon, France, bernard.normand@insa-lyon.fr*

Abstract:

The corrosion of 2205 duplex stainless steel (DSS) could occur in atmospheric distillation column and overhead condensation systems of refinery plant due to the combined affection of hydrochloric acid and hydrogen sulfide when temperature is below the dew point.

In this paper, the effects of sulfide on the corrosion behaviour of 2205 DSS in HCl solutions were investigated using mass loss tests, potentiodynamic polarization tests, electrochemical impedance spectra, scanning Kelvin probes, scanning electron microscopy and X-ray photoelectron spectroscopy. The results showed that Na_2S had a significant effect on the corrosion behaviour of 2205 DSS in dilute HCl solutions. Low levels of S^{2-} can protect the passive film of 2205 DSS from localized attack by Cl^- in HCl solution with concentrations lower than 0.1 mol/L. In comparison, when the HCl solution concentration is higher than 0.137 mol/L, Na_2S addition will greatly promote the corrosion of 2205 DSS. Additionally, SEM images revealed that the addition of Na_2S resulted in intergranular corrosion with deep micro-cracks of the 2205 DSS in HCl solutions. The combination effect of H^+, Cl^-, S^{2-} and HS^- would accelerate the active corrosion remarkably when concentrations of hydrochloric acid and Na_2S were high enough at the same time. The detailed corrosion mechanism of 2205 DSS in investigated media was proposed in this work as well.

Keywords:

Duplex stainless steel, HCl, Na_2S, EIS, XPS

Introduction

In the oil and gas industry, the corrosion situation has worsened with the increasing quantities of sulfide, chloride and carbon dioxide in crude oil [1, 2]. This is most notable in atmospheric distillation columns and overhead condensation systems, which are the primary equipment types directly subject to corrosion risk from the detrimental contents of crude oils even after the desalting and dehydration processes [3, 4]. In these systems, corrosion occurs due to the combined action of the hydrochloric acid formed by the hydrolysis of chlorine salt or organic chloride and the hydrogen sulfide contained in the crude oils [5–8]. 2205 duplex stainless steels (DSS) have become promising candidate materials for use in these systems due to their excellent mechanical behaviour and high corrosion resistance [9–11].

In particular, the effects of chloride or sulfide on the corrosion of DSS have attracted intense attention. Jeon et al. [12] demonstrated super DSS in a NaCl solution at pH 7 showing some pitting corrosion and in a NaCl + HCl solution at pH 1 showing uniform corrosion plus pitting. It was also revealed that ferrite phase was uniformly corroded to a greater extent than austenite phase was due to their different corrosion resistances in chloride solutions. Wan et al. [13] focused on the effect of chloride ions on the corroded surface layer of 00Cr22Ni5Mo3N duplex stainless steel under cavitation. They proved that Cl^- had a strong effect on the nano-mechanical parameters of the corroded surface layer of DSS and promote preferential dissolution of ferrous oxides and reduce the ability of passive film. Dong and Luo et al. [14] reported the spontaneously passivation behaviours and pitting corrosion of 2205 DSS in chloride solutions. It was demonstrated that the temperature and concentration of the chloride played important roles in altering the thickness of the passive film and the shape of the pits. Lo et al. [15] studied the selective dissolution of 2205DSS between two phase in HCl solution. The result is that with increasing concentration of HCl, austenite phase dissolution was faster than ferrite phase dissolution. Liu et al. [16] studied the stress crack corrosion of 2205DSS in CO_2-H_2S condition, they suggested that presence of H_2S can primarily result in the reduction of H^+ and the oxidation of steel to form FeS in the solution of pH lower than 3. Also, the passive current density of 2205 DSS increases with the decrease in solution pH. Liu et al. [17] reported that 2205 DSS was highly susceptible to sulfide stress corrosion cracking (SSCC) as pH decreased and H_2S concentration increased. The proposed mechanism was the cathodic reaction could be accelerated by H_2S in low pH H_2S-contain solution, which leaded fast breakdown of passive film by H^+ reduction and Cl^- attacking. In addition, the boundary of the ferrite phase and austenite phase promoted the initiation of SSCC, while the austenite phase inhibited its propagation.

However, the corrosion behaviours of 2205 DSS in HCl solution with sulfide at high temperature have received little attention. Although some researchers have performed many studies on the combined effects of chloride and sulfide, their studies mainly focused on carbon steel and austenite steels [18–21]. Further research work on the corrosion mechanism of 2205 DSS in HCl + H_2S solution, which often occurs in atmospheric distillation columns and overhead condensation systems, is still necessary.

This work aimed at providing an improved understanding of the corrosion process and mechanism of 2205 DSS in a simulated solution of HCl plus Na_2S, representing the aqueous medium in atmospheric distillation columns and overhead condensation systems. The corrosion behaviours of 2205 DSS in HCl plus Na_2S solutions were compared through

studying their mass loss, polarization curves and electrochemical impedance spectra (EIS), Kelvin potential distribution mappings, micromorphologies and surface compositions.

Experimental details

Mass loss test experiments

The 2205 DSS specimens were cut into 40 mm × 15 mm × 2 mm. The chemical composition (wt.%) of 2205 DSS was C 0.03, Si 1.00, Mn 2.00, P 0.03, S 0.02, Ni 4.80, Cr 22.00, Mo 3.00, N 4.80 and balance Fe. The specimens were sequentially ground with 2000 grit SiC paper, degreased with acetone and alcohol, cleaned in water and dried in air.

The corrosion rates of 2205 DSS were measured after 8 hours immersion at 90°C in HCl solutions with concentrations of 0.548, 0.274, 0.137, 0.1, 0.01 and 0.001 mol/L in the absence and presence of 0.385 mmol/L Na_2S. The resulting corrosion rates R (mm/a) were calculated by the following formula:

$$\boldsymbol{R} = \frac{(\boldsymbol{M_1}-\boldsymbol{M_2})\cdot\mathbf{87600}}{\mathbf{S}\cdot\mathbf{T}\cdot\boldsymbol{\rho}} \qquad (1)$$

where S (cm^2), M_1 (g), M_2 (g), T (h) and ρ (g/cm^3) represent the specimen surface area, the specimen weight before and after the test, the length of the test and the specimen density, respectively.

Electrochemical experiments

Open circuit potential (OCP), EIS and polarization curve measurements were performed in a conventional three-electrode cell by using a CS350 (CorrTest, Wuhan, China) electrochemical test system. The ground specimens used as the working electrode were made of 1 cm × 1 cm high-temp RTV silicone. A saturated calomel electrode (SCE) was used as the reference electrode. A platinum foil electrode was used as the counter electrode. All potentials were measured against SCE.

After 1 hour of OCP measurement, EIS was performed in a frequency range from 100 kHz to 0.01 Hz with an applied AC amplitude of 10 mV (vs. OCP). Then, the polarization curves were recorded by dynamic potential scanning using a scan rate of 0.5 mV/s and starting from -0.1 V (vs. OCP). The test stopped when the polarization current density reached 1 $mA\cdot cm^{-2}$. The impedance data were fitted with ZsimpWin software using equivalent circuits.

Scanning Kelvin probe

The potential maps of 2205 DSS samples before and after immersion in 0.137 mol/L HCl + 0.385 mmol/L Na_2S solution were recorded by an scanning Kelvin probe (SKP) technique. The experiments were performed on a VersaScan electrochemical scanning system (Princeton Applied Research, Ametek). All specimens used in SKP test were polished with polishing machine, using Al_2O_3 abrasive grain (0.1 μm grade). All tests were performed at the same ambient temperature and relative humidity. Step scan mode was employed, with a step size of 20 μm and a scan area of 1000 μm × 1000 μm.

SEM and XPS analysis

The microstructures of 2205 DSS specimens with or without corrosion products were observed with an EVO MA15 (Carl Zeiss Jena, Germany) scanning electron microscope

(SEM). The chemical composition of the 2205 DSS surface was analysed with an X-ray photoelectron spectrometer (XPS) (ESCALAB 250, ThermoFisher Scientific, USA) using 150 W monochromatic Al Kα as the radiation source with an energy of 200 eV and a pass energy of 30 eV. The splitting and fitting of overlapped peaks were performed with Xpspeak4.1 commercial software, which contained Shirley background subtraction and Gaussian Lorentzian tail functions for better spectral fitting.

Results

Mass loss test

Fig. 1 shows the corrosion rates of 2205 DSS in different concentrations of HCl solution with or without 0.385 mmol/L Na_2S at 90°C for 8 hours. Two vertical coordinates are presented in Fig. 1, one is corrosion rate, and the other is growth ratio, which is defined as the ratio of the corrosion rates in the presence and absence of 0.385 mmol/L Na_2S. The corrosion rate slightly decreased in HCl solutions at concentrations below 0.137 mol/L with Na_2S addition, indicating that Na_2S has a corrosion inhibition effect at appropriate concentrations. In 0.137 mol/L and 0.274 mol/L HCl solutions without Na_2S, the corrosion rates of 2205 DSS were 0.0114 mm/a and 0.0130 mm/a, respectively. However, the presence of 0.385 mmol/L Na_2S in such solutions increased the corrosion rates of 2205 DSS remarkably. They increased to 12.364 mm/a and 24.506 mm/a, respectively. Meanwhile, the growth ratios accordingly increased to 108549% and 188550%. As 2205 DSS was exhibiting active dissolution, the corrosion rates in 0.548 mol/L HCl with and without Na_2S increased to 52.734 mm/a and 81.252 mm/a, and the growth ratio declined to 54%.

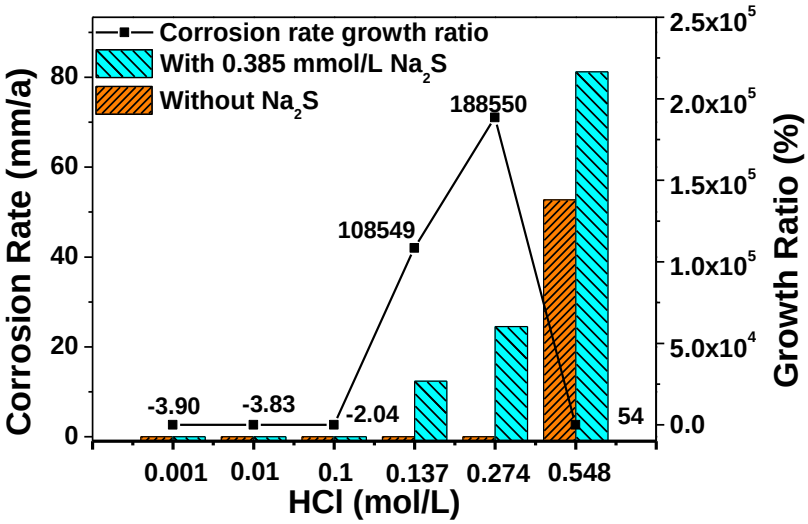

Fig. 1 Corrosion rates of 2205 DSS in different concentrations of HCl solution with or without Na_2S at 90 ℃.

The above results show the interesting corrosion behaviour of 2205 DSS in dilute HCl solutions caused by the presence of Na_2S. With the addition of Na_2S, the critical HCl concentration for active dissolution corrosion of 2205 DSS reduces from 0.548 mol/L to 0.137 mol/L.

Polarization curves measurement

Fig. 2 shows polarization curves of 2205 DSS in HCl solutions both without and with

different concentrations of Na_2S at 90°C. Generally, in aerated, dilute HCl solution, 2205 DSS can passivate spontaneously, and the cathodic reaction is dissolved oxygen reduction. However, Cl^- has a strongly destructive effect on passive films [23, 24], and hence, the stability of the passive film of 2205 DSS could be greatly influenced by Cl^- attacking. As shown in Fig. 2a, with the increase in HCl concentration, the corrosion potential shifts more negatively, and the passivation current density increases. Meanwhile, with the increase in HCl concentration, the passive region narrows and the breakdown potential decreases. The first significant change occurs in 0.137 mol/L HCl solution, where the breakdown potential of the passive film drops suddenly at approximately 0.3 V. Since the sample is still in the passivation state, hydrogen depolarization reactions could be ignored. This result indicates that 0.137 mol/L HCl solution are very detrimental to the stability of the passive film of 2205 DSS, which might be relative to the significant change happens in the same concentration in the mass loss test when Na_2S is added. The second significant change occurs in 0.548 mol/L HCl solution, where two free corrosion potentials are found in the polarization curve of 2205 DSS. These can be ascribed to the current oscillation phenomenon caused by the active-passive transition of 2205 DSS in higher concentration HCl solutions, as previously studied [24]. It is in accordance with the active dissolution corrosion concentration in mass loss test. From the results of Fig. 1 and Fig. 2a, it can be revealed that 0.137 mol/L is the critical concentration for the passivation behaviour of 2205 DSS in HCl solution at 90°C.

Fig. 2b shows the polarization curves for 2205 DSS in 0.1 mol/L HCl solution (lower than the critical concentration 0.137 mol/L) with Na_2S from 0 to 3.846 mmol/L. With the addition of Na_2S, the corrosion potential is more positive than without Na_2S, indicating that Na_2S can significantly affect the cathodic corrosion reaction. The passivation current density increases and the breakdown potential decreases with the increase in Na_2S when its concentration is above 0.385 mmol/L. A possible reason for this is that sulfide ion can inhibit OH^- or O_2 from adsorbing onto the metal surface to obstruct the regeneration of the passive film [25].

Fig. 2c shows the polarization curves of 2205 DSS in 0.137 mol/L HCl solutions with Na_2S from 0 to 0.385 mmol/L. When adding 0.128 mmol/L and 0.256 mmol/L Na_2S in solution, the corrosion potential moves positively, the passivation region enlarges and the passivation current density maintains similar values, suggesting that localized corrosion is inhibited by S^{2-} ion [26]. However, the corrosion potential rapidly decreases and the anodic current densities increase greatly when the concentration of Na_2S increases to 0.385 mmol/L, affirming the corrosion process is tremendously promoted by Na_2S and 2205 DSS cannot passivate anymore.

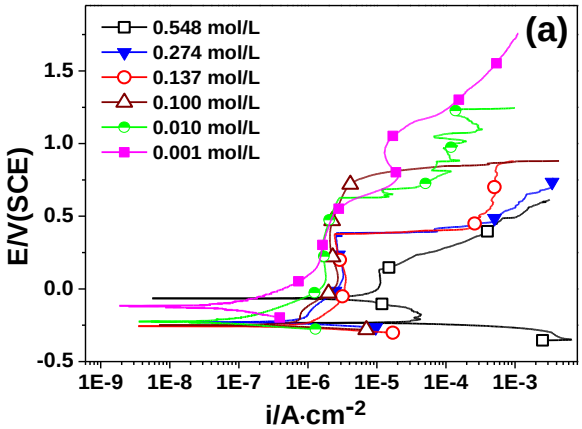

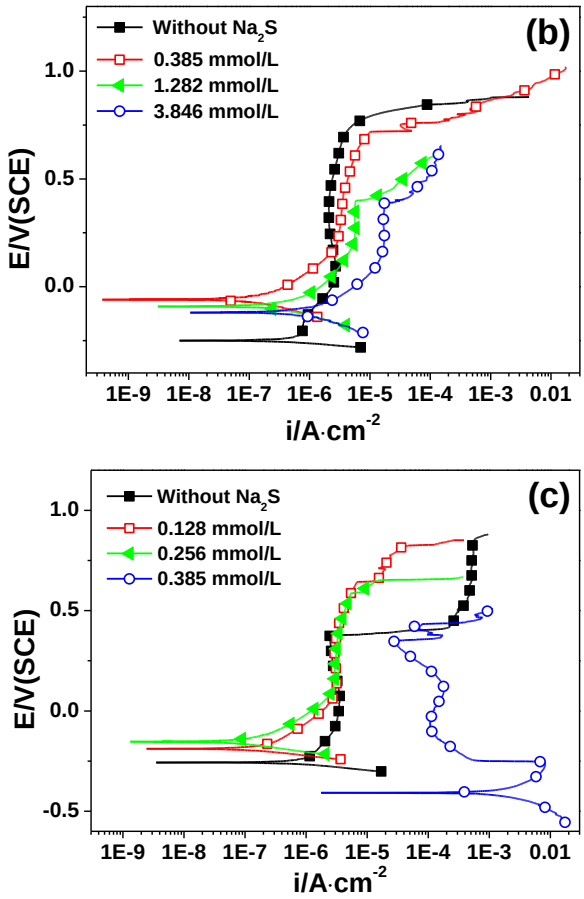

Fig. 2 Polarization curves of 2205 DSS in (a) HCl solutions, (b) 0.1 mol/L HCl + Na_2S solutions and (c) 0.137 mol/L HCl + Na_2S solutions at 90 ℃.

EIS study

To understand the electrochemical kinetic information at the interface, Fig. 3 shows the Nyquist plots from the EIS measurement. In brief, the capacitive semicircle at high frequency is related to the corrosion product film or passive film on the metal surface, while the capacitive semicircle at low frequency is associated with the double layer capacitance and charge transfer resistance [25]. As shown in Fig. 3a, when the concentration of HCl is higher than 0.01 mol/L, the Nyquist plots present a double capacitive semicircle that exhibits two distinct time constants, indicating an incomplete passivation state on the surface of the 2205 DSS [28, 29]. With lower concentrations of HCl (0.001 and 0.01 mol/L), the capacitive semicircle extends at high frequency, and the Nyquist plots tend to be more smooth, which implies more intact passive film on the surface of 2205 DSS [29]. It is clear that the corrosion resistance of 2205 DSS decreases with the increase in HCl concentration.

Fig. 3b shows Nyquist plots of 2205 DSS in 0.1 mol/L HCl solutions with different concentrations of Na_2S. The capacitive semicircle of the Nyquist plots becomes much larger with the presence of 0.385 mmol/L Na_2S, indicating the improvement of corrosion resistance. However, the diameter of the capacitive semicircle decreases with the increase in Na_2S from 0.385 to 3.846 mmol/L, indicating that the corrosion resistance of 2205 DSS decreases with the increase in Na_2S concentration.

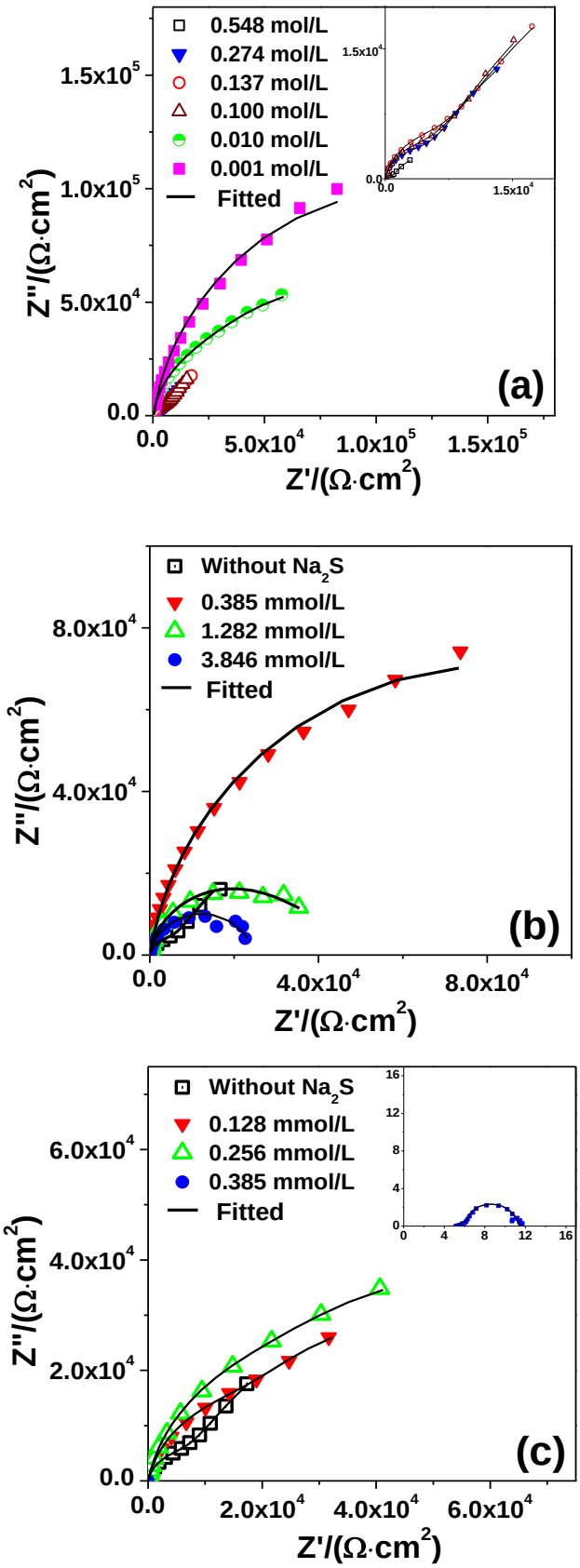

Fig. 3 Nyquist plots and the fitting curves for 2205 DSS in (a) HCl solutions, (b) 0.1 mol/L HCl+ Na_2S solutions and (c) 0.137 mol/L HCl+ Na_2S solutions at 90 ℃.

Fig. 3c shows Nyquist plots of 2205 DSS in 0.137 mol/L HCl solutions with different

concentrations of Na_2S. The shapes of the capacitive semicircle of the Nyquist plots are altered from that of the blank solution by adding 0.128 and 0.256 mmol/L Na_2S, which demonstrates that the corrosion kinetics of 2205 DSS are affected by the presence of trace S^{2-} ions. However, when the concentration of Na_2S reaches 0.385 mmol/L, the active dissolution of 2205 DSS occurs such that the capacitive semicircle of the Nyquist plots shrinks dramatically. These results accord perfectly with the mass loss and polarization curve results.

To further analyse the kinetic parameters affected by S^{2-} addition, an equivalent circuit as shown in Fig. 4 was applied to fit the EIS data. This equivalent circuit has two time constants. In the first process at higher frequency, the constant phase element parameter CPE_1 represents the capacitive behaviours of the passive film, and R_1 is the film resistance, which demonstrates the resistance of the ionic paths through the oxide film. In the second process, detected at low frequency, constant phase element CPE_2 represents the capacitive behaviour, and R_2 represents the corresponding charge-transfer resistance [31, 32] of the electrochemical reaction at the metal/solution interface. The EIS fitting results of 2205 DSS in 0.1 and 0.137 mol/L HCl solutions with different addition of Na_2S are listed in Table 1.

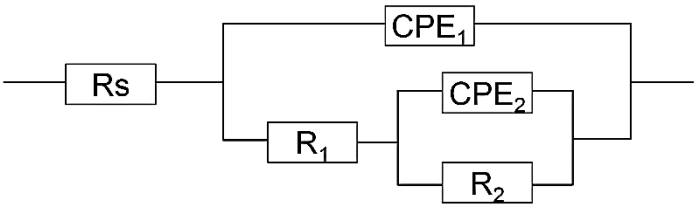

Fig. 4 Equivalent circuit for fitting.

Table 1. EIS fitting data of 2205 DSS in HCl solutions with different [Na_2S] at 90°C

HCl (mol/L)	Na_2S (mmol/L)	Rs (Ω cm^2)	CPE_1 ($\mu\Omega^{-1}cm^{-2}s^n$)	n	R_1 (kΩ cm^2)	CPE_2 ($\mu\Omega^{-1}cm^{-2}s^n$)	n	R_2 (KΩ cm^2)
0.100	0	9.67	71.71	0.89	11.04	278.70	0.80	109.70
	0.385	7.94	62.81	0.90	13.12	4.43	0.80	155.90
	1.282	7.35	60.21	0.90	36.78	1103.00	0.80	10.60
	3.846	6.97	66.58	0.88	22.86	3746.00	0.80	1.50
0.137	0	5.99	75.01	0.89	10.33	266.40	0.80	91.02
	0.128	5.82	79.34	0.87	35.11	336.10	0.80	44.36
	0.256	5.54	80.47	0.87	56.16	318.00	0.97	41.44
	0.385	5.41	5545.00	0.80	0.0012	9038.00	0.97	0.0048

From Table 1, the film resistance R_1 is improved in the 0.1 mol/L HCl solution by adding

Na_2S, revealing an enhancement of the passive film. In 0.1 mol/L HCl solution with 0.385 mmol/L Na_2S addition, it is interesting to note that CPE_2 decreases and resistances (R_1 and R_2) increases compared to those values in the solution without Na_2S. The result clearly shows that it is possible to inhibit the corrosion of 2205 DSS by adding a small quantity of Na_2S. However, after adding Na_2S, CPE_2 increases and R_2 decreases with the increase in Na_2S concentration, indicating the promotion of the charge-discharge process of the double layer related to anodic dissolution and cathodic reduction. The total resistance (R_1 + R_2) representing the overall corrosion reaction resistance decreases with increasing Na_2S content, and it becomes much lower in 0.1 mol/L HCl solution when the Na_2S concentration reaches 1.282 mmol/L.

For 2205 DSS in 0.137 mol/L HCl solution without Na_2S, R_1 and R_2 both decrease slightly compared with that in 0.1 mol/L HCl. By adding Na_2S from 0.128 to 0.256 mmol/L, the film resistance R_1 rises with the increase in Na_2S concentration. However, the total resistance (R_1 + R_2) is reduced slightly by Na_2S addition, as charge transfer resistance R_2 decreases greatly. As a result, no corrosion inhibition effect of Na_2S could be observed in the 0.137 mol/L HCl solution at corrosion potential. Finally, in 0.137 mol/L HCl + 0.385 mmol/L Na_2S solution, CPE_1 and CPE_2 increase remarkably while R_1 and R_2 drop dramatically, corresponding to the active dissolution of 2205 DSS. In summary, the electrochemical behaviour of 2205 DSS in 0.137 mol/L HCl with Na_2S is quite different from that of 2205 DSS in 0.1 mol/L HCl with Na_2S.

Scanning Kelvin probe mapping

Fig. 5 shows the 3D surface potential mappings of the same area on the 2205 DSS surface before and after immersion in 0.137 mol/L HCl + 0.385 mmol/L Na_2S solution for 20 s. In Fig. 5a, higher surface potential presents in the top region and lower surface potential presents in the bottom region of the original 2205 DSS surface, probably corresponding to austenite and ferrite phases, respectively, as the ferrite phase is less noble in duplex stainless steel [32].

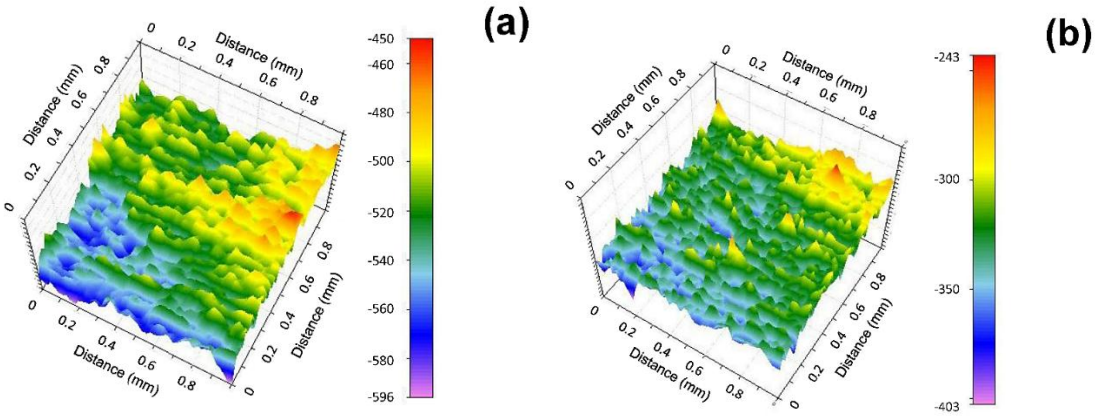

Fig. 5 Surface potential 3D mappings of 2205 (a) before and (b) after immersion for 20 s in 0.137 mol/L HCl + 0.385 mmol/L Na_2S solution.

After immersion, the anodic region is much larger than before (Fig. 5b), which indicates that the corrosive medium has very rapidly changed the surface state significantly. Meanwhile, the potential range also enlarges after immersion, as presented in Table 2. According to SKP analysis, this result demonstrates that the surface becomes active and that corrosion occurs on

most regions of the surface from the beginning.

Table 2 Potential variation range in SKP mapping

Samples (2205 DSS)	ΔE_{SKP} (mV)
Before immersion	146
After immersion	160

Corrosion micro-morphology

The metallographic images of the specimens obtained by metallographic microscope are shown in Fig. 6. Before metallographic observation, the specimen is etched with solution (36 wt.% HCl: anhydrous ethanol =1:1) in the presence of 2.5 g/L $CuCl_2$ after polishing. In Fig. 6a, the light-coloured area is austenite phase, the dark area is ferrite phase, and the distribution of phases is relatively uniform. Fig. 6b gives the metallographic image of the corrosion micro-morphology on 2205 DSS after immersion for 4 hour in 0.137 mol/L HCl + 0.385 mmol/L Na_2S solution. There are many dark spots corresponding to the most corroded regions, and the corrosion along the grain boundaries is more severe.

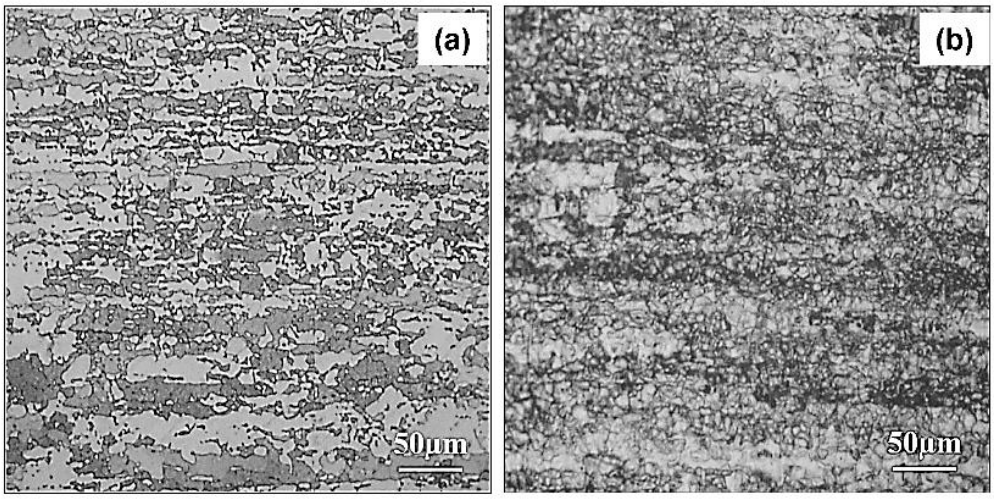

Fig. 6 Metallographic images of 2205 DSS (a) before and (b) after 4 hours of corrosion in 0.137 mol/L HCl + 0.385 mmol/L Na_2S solution, corrosion product was removed.

The SEM images of 2205 DSS after mass loss experiments in HCl and HCl + Na_2S solutions are shown in Fig. 7. Fig. 7a shows that pitting corrosion occurs on 2205 DSS in 0.1 mol/L HCl solutions. More corrosion defects (larger pits) can be observed when the concentration of HCl is elevated to 0.137 mol/L HCl solution, as shown in Fig. 7b. It is apparent that the corrosion is more severe in the 0.137 mol/L HCl solution. It seems that the different degrees of corrosion in pure HCl solutions essentially determine the corrosion behaviour of 2205 DSS in the HCl + Na_2S solutions. As shown in Fig. 7c, only two pits were found on 2205 DSS when adding 0.385 mmol/L Na_2S in 0.1 mol/L HCl solutions, and the pit size decreased compared with that in Fig. 7a. The corrosion of 2205 DSS is enhanced in 0.1 mol/L HCl + 3.846 mmol/L Na_2S (Fig. 7d). There are many corrosion pits on the surface, however, no dramatic acidic corrosion was promoted. As shown in former results of this paper, the corrosion behaviour of 2205 DSS is quite different in 0.137 mol/L HCl solution with Na_2S. Despite 0.128 mmol/L Na_2S preventing the corrosion of 2205 DSS (Fig. 7e) in 0.137 mol/L

HCl solution, 0.385 mmol/L Na_2S can remarkably promote the corrosion (Fig. 7f). In addition, many deep holes under the corrosion product film can be observed in the cross-sectional sample image in Fig. 7f. These results indicate that both general and localized corrosion exist in such conditions. The corrosion morphology in 0.548 mol/L HCl (Fig. 7g) looks the same as in Fig. 7f. Both surfaces of the corroded samples are covered by loose corrosion-product films. The corrosion micro-morphology of the 2205 DSS with and without Na_2S after removing the corrosion products are shown in Fig. 7h and Fig. 7i, respectively. In good agreement with Fig. 7f, there are many micro-defects in the 2205 DSS surface under the corrosion product film after immersion in 0.137 mol/L HCl + 0.385 mmol/L Na_2S solution (Fig. 7h). It is clear from Fig. 7f, the morphology of these defects also include crack besides of pit, in fact. These corrosion defects are likely to occur on grain boundaries of austenite and ferrite, while no such corrosion defects are observed on the surface of 2205 DSS after immersion in 0.548 mol/L HCl solution (Fig. 7i). Only a general corrosion morphology of acidic corrosion is presented in Fig. 7i. Hydrogen-induced cracking (HIC) of low alloy steel or stainless steel is often found in the corrosion of H_2S-containing solutions [33]. A similar mechanism might be present in this investigation. However, these micro-defects presented Fig. 7f and Fig. 7h do not look like typical HIC cracks. Furthermore, no selective corrosion of the austenite phase or the ferrite phase is observed in micro-morphology characterization.

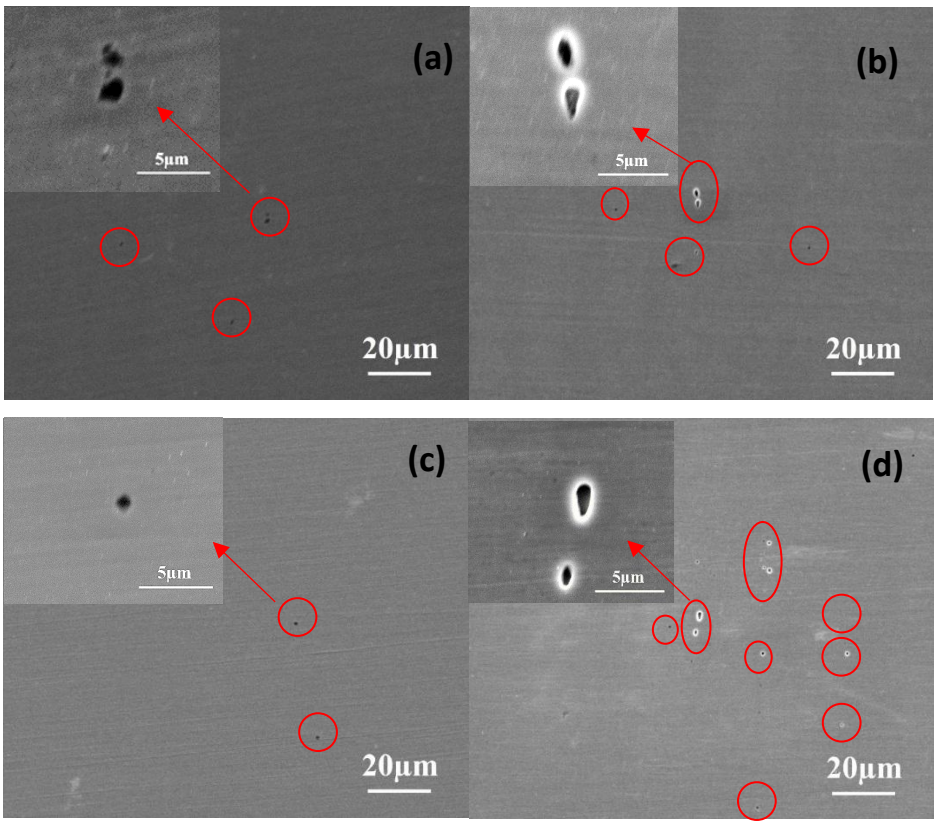

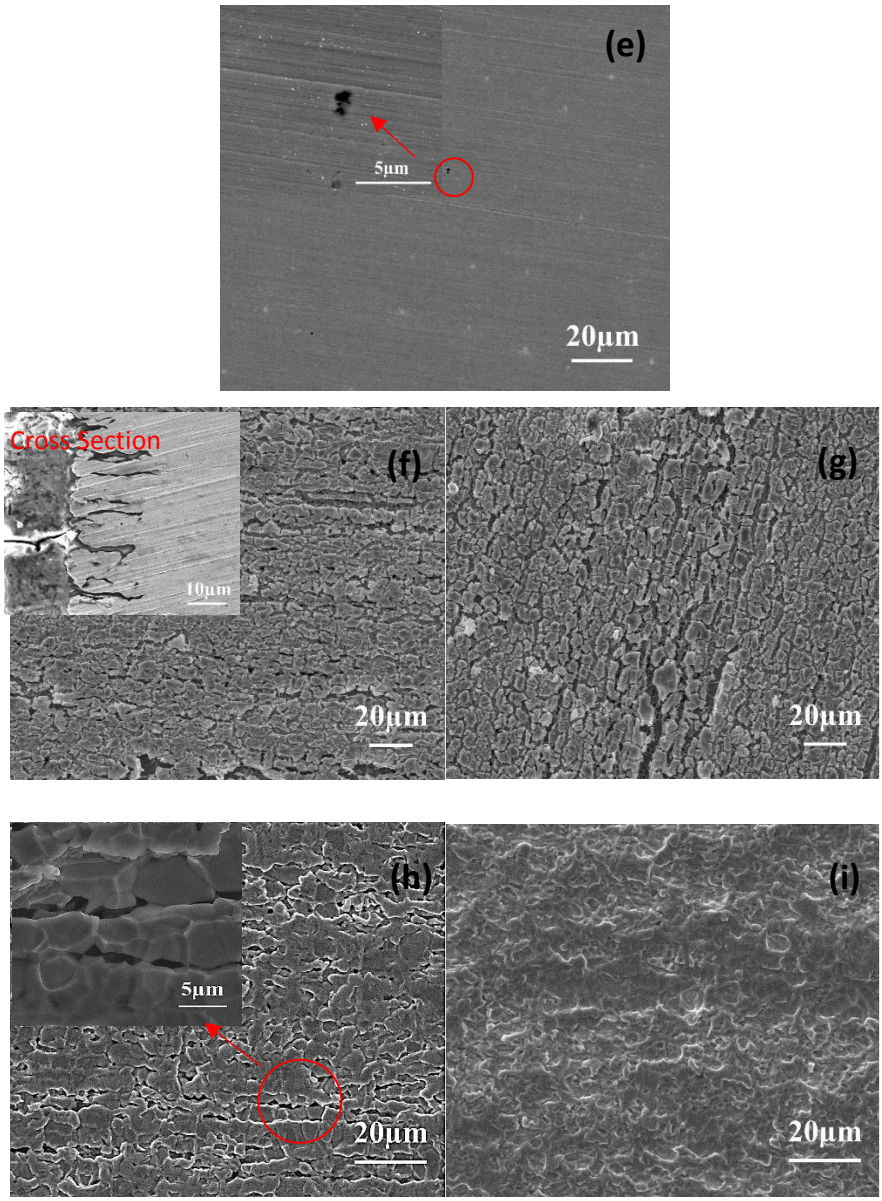

Fig. 7 Corrosion micro-morphology SEM images of 2205 DSS after 8 hours of immersion in (a) 0.1 mol/L HCl, (b) 0.137 mol/L HCl, (c) 0.1 mol/L HCl + 0.385 mmol/L, (d) 0.1 mol/L HCl + 3.846 mmol/L, (e) 0.137 mol/L HCl + 0.128 mmol/L, (f) 0.137 mol/L HCl + 0.385 mmol/L Na_2S, (g) 0.548 mol/L HCl, and (h) without corrosion product film 0.137 mol/L HCl + 0.385 mmol/L, (i) without corrosion product film 0.548 mol/L HCl.

XPS analysis

Fig. 8a shows the large scale XPS spectra of the passive films on the 2205 DSS surface after immersion in 0.137 mol/L HCl and 0.137 mol/L HCl + 0.128 mmol/L Na_2S solution at 90°C for 8 hours. For both samples, only Cr, Fe, Mo, Ni and O are detected on their surfaces. Fig. 8b shows the large scale XPS spectrum of the 2205 product film in 0.137 mol/L HCl + 0.385 mmol/L Na_2S solution at 90°C for 8 hours. It is clear that the corrosion product on the surface is mainly composed of Mo, Cr, Ni, O, S and trace Cl.

Fig. 9 shows the high-resolution scanning XPS spectra for each element found in the two passive films. The Cr 2p spectrum can be separated into several constituent peaks of Cr,

Cr_2O_3 and $Cr(OH)_3$. The intensities of the Cr_2O_3 peaks are higher than those of $Cr(OH)_3$ and metallic Cr. They are also the highest of all the constituent peaks in two passive films. Thus, Cr_2O_3 is the primary constituent of the passive films on 2205DSS. The Fe 2p spectrum reflects the existence of metallic Fe, Fe_2O_3 and Fe_3O_4 in the passive film. The overlapping peaks of Mo 3d reveal that metallic Mo, Mo^{4+} and Mo^{6+} exist in the passive film. The Ni 2p spectrum shows three constituent peaks, respectively representing metallic Ni and NiO. The O 1s peaks in two passive films both can be split into three components, O^{2-}, OH^- and bound H_2O. From the above observations, both two passive films are mainly composed of the oxides and hydroxides of Cr, Mo, Ni and Fe, the same as the previously investigation in sodium thiosulphate solution [34]. That is to say, the addition of a low content S^{2-} would not change the chemical composition of the passive film on 2205DSS in HCl based solution.

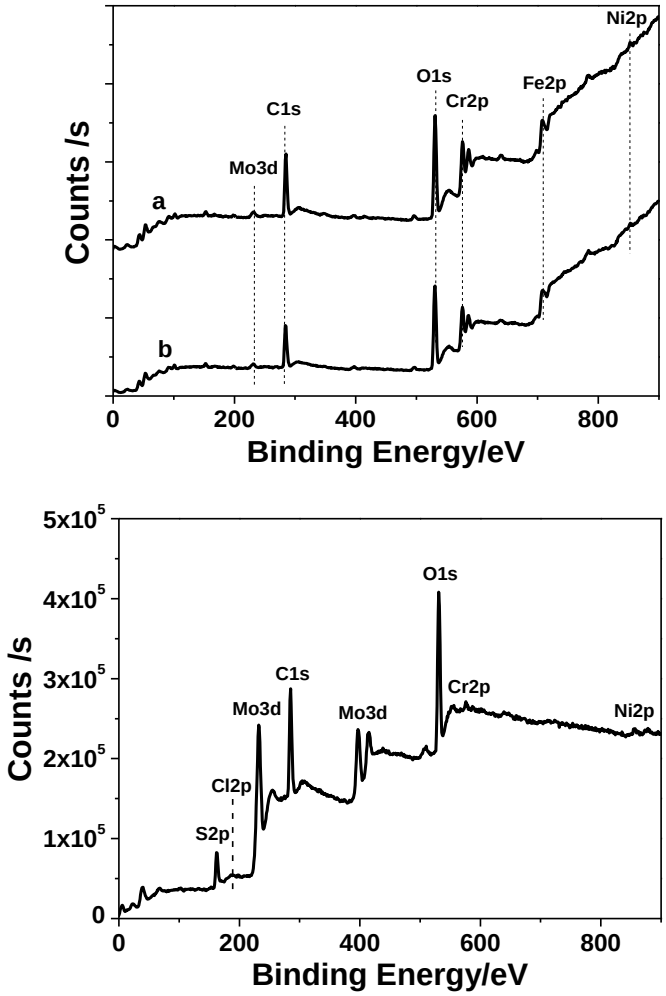

Fig. 8 Large scale scanning XPS spectra of (a) passive films on 2205 DSS surface in 0.137 mol/L HCl solution and 137 mol/L HCl solution with 0.128 mmol/L Na_2S, (b) corrosion product film on 2205 DSS surface in 137 mol/L HCl solution with 0.385 mmol/L Na_2S.

Fig. 10 shows the high-resolution scanning XPS spectra for each element found in the corrosion products. The XPS peaks are separated into different combined states referring to XPS analysis of similar corrosion products [35] by a fitting procedure that is described in the experimental section. Fe 2p cannot be detected, possibly because iron can easily dissolve into acidic solution without existing in the corrosion product film. The chromium peak can split

into three peaks corresponding to Cr_2O_3 and $CrCl_3$, as shown in Fig. 10a. According to Fig. 10b, a good deal of molybdenum exists in the corrosion products, in the forms of Mo^{4+} and Mo^{6+}. A small amount of nickel can be observed in Fig. 10c, probably present in oxide, hydroxide and chloride forms. The spectrum of S 2p shown in Fig. 10d presents two constituents of S^{2-} in the corrosion products, indicating that sulfide ions from Na_2S addition have taken part in the corrosion reactions and that different metal sulfides were formed. The mechanism of the sulfide ion role in the corrosion process will be discussed in the following section. In Fig. 10e, peaks of O 1s correspond to O^{2-} and OH^-, which refer to the presence of Cr_2O_3, NiO, and $Ni(OH)_2$. The Cl 2p peaks in Fig. 10f correspond to the $NiCl_2$ and $CrCl_3$. The above results reveal that the corrosion products are mainly composed of metal (except Fe) oxides and/or hydroxides, sulfides and chlorides.

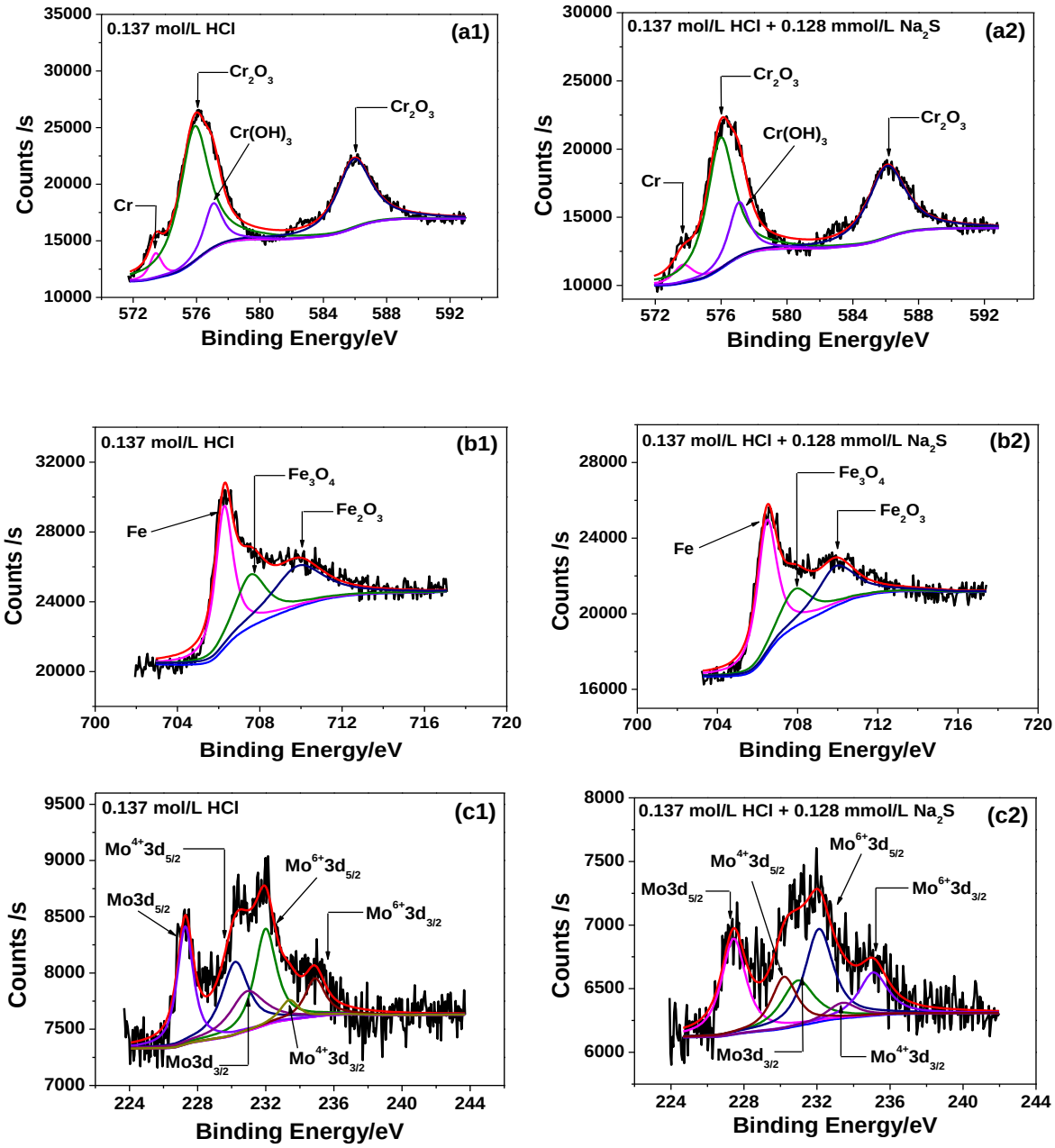

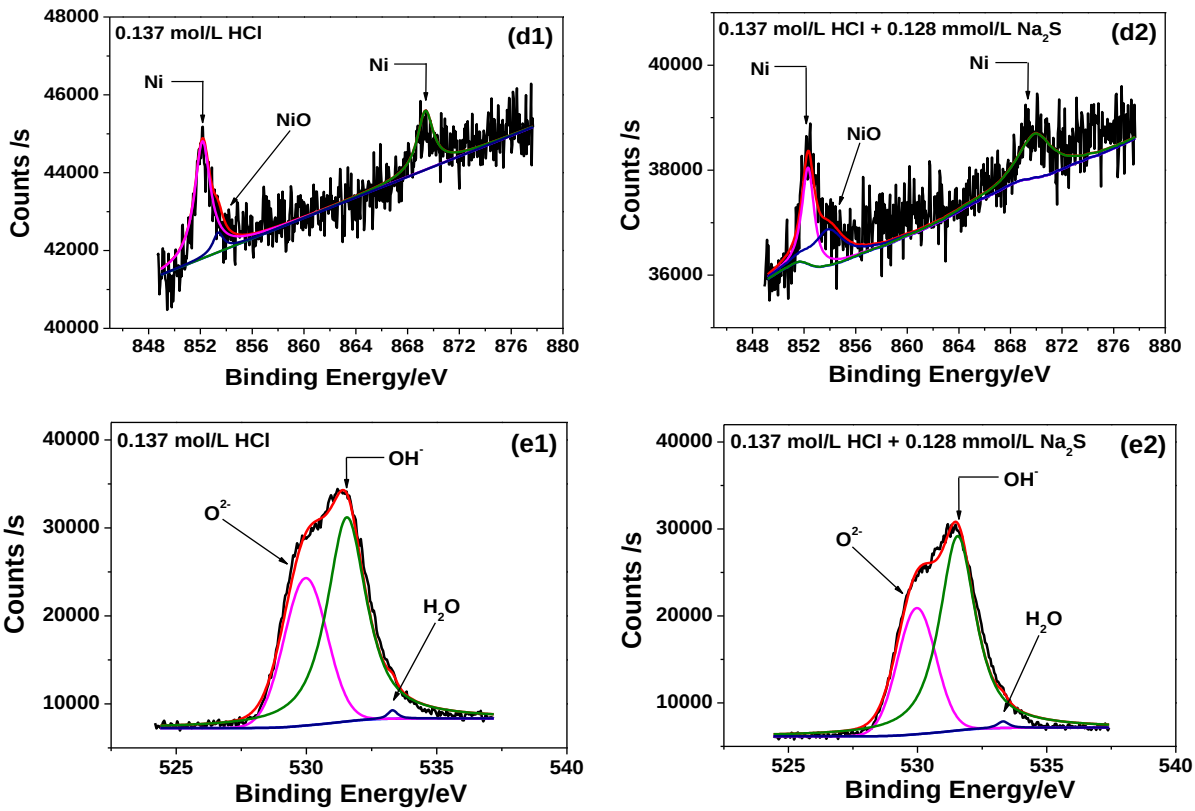

Fig. 9 High-resolution scanning XPS spectra of (a) Cr 2p, (b) Fe 2p, (c) Mo 3d, (d) Ni 2p and (e) O1s in passive films on 2205 DSS surface in solutions of 0.137 mol/L HCl and 0.137 mol/L HCl with 0.128 mmol/L Na_2S.

Fig. 11 shows the atomic fraction of each element in the surface films of 2205 DSS under different states. The atomic fractions of all the elements in the passive film show no distinct differences in the 0.137 mol/L HCl solution and the 0.137 mol/L HCl + 0.128 mol/L Na_2S solution. However, the composition of the corrosion product film in 0.137 mol/L HCl + 0.385 mol/L Na_2S solution exhibits a significant increase in molybdenum content and decrease in chromium content compared with those in the passive film. This is because atomic molybdenum has greater difficulty reacting with hydrochloric acid (dissolution reaction) compared to other metallic elements but can react with H_2S or dissolved oxygen in acidic solution to form molybdenum sulfide, oxides and/or hydroxides, which are also stable in dilute HCl solution.

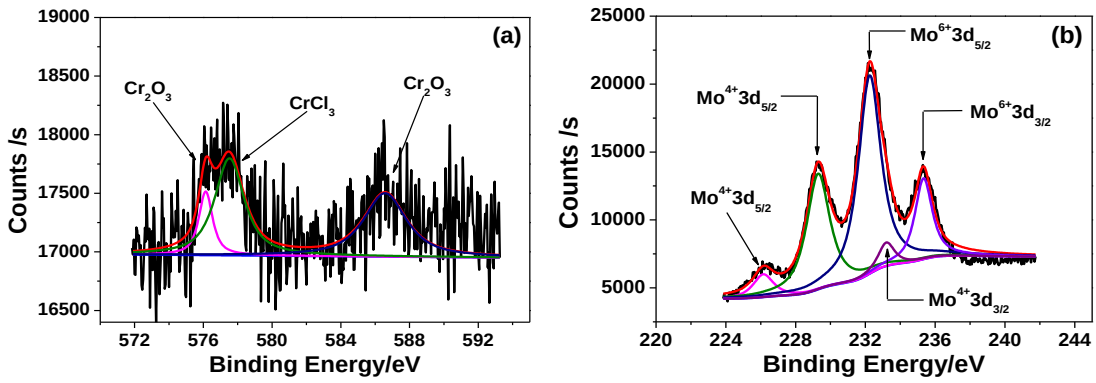

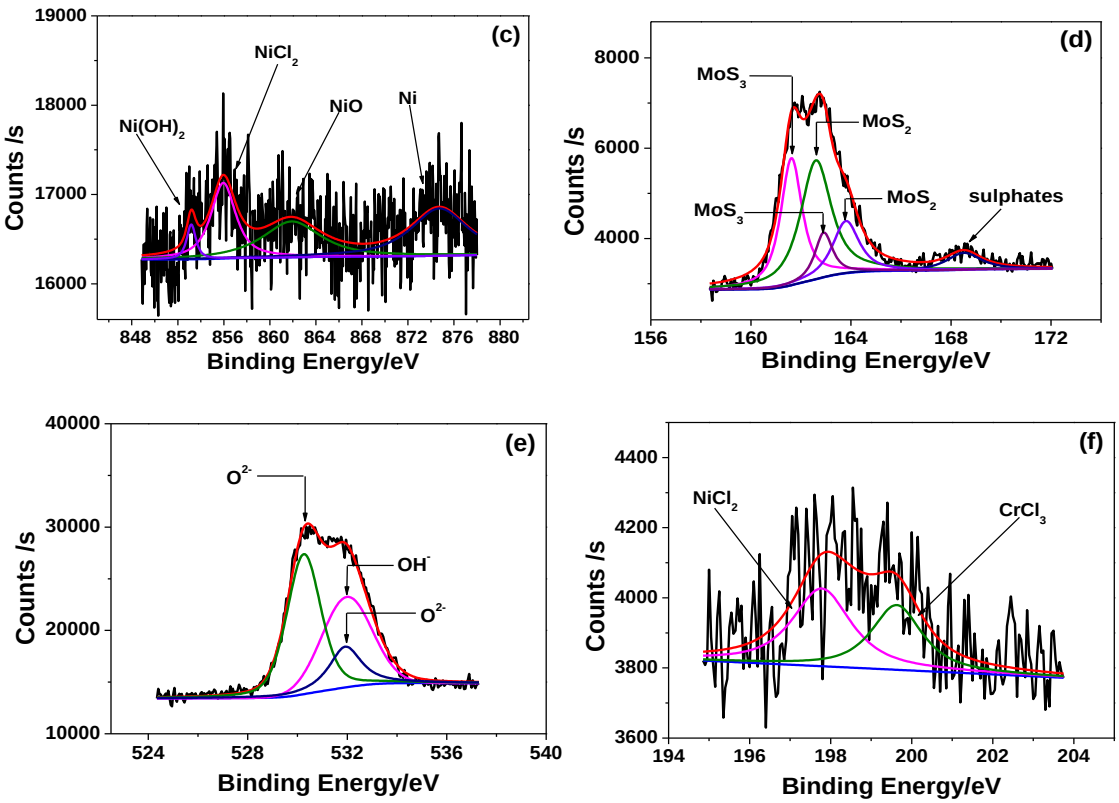

Fig.10 XPS spectrum of (a) Cr 2p, (b) Mo 3d, (c) Ni 2p, (d) S 2p, (e) O 1s and (f) Cl 2p in corrosion product film on 2205 DSS surface in 137 mol/L HCl solution with 0.385 mmol/L Na_2S.

In summary, the passive film is mainly composed of Cr(III) oxide-hydroxides with high chemical stability, which offers excellent protection for the 2205 DSS matrix. In contrast, once the active dissolution of 2205 DSS occurs in 0.137 mol/L HCl + 0.385 mol/L Na_2S solution with strong acidic and reductive properties at high temperature, the possible intermediate products of ferrous oxide or sulfide would not exist during dissolution, and the surficial chromium oxides would not be sufficient for blocking corrosion.

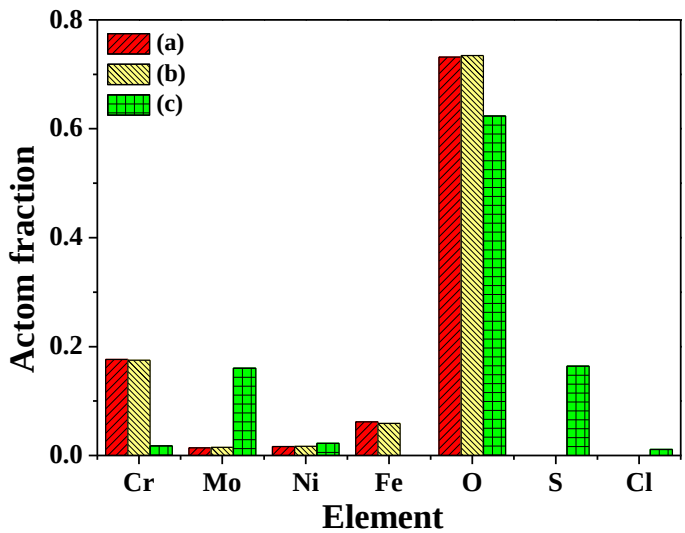

Fig. 11 Atom fraction of elements in surficial films of 2205 DSS: (a) passive film in 0.137 mol/L HCl solution, (b) passive film in 0.137 mol/L HCl + 0.128 Na_2S solution, (c) corrosion

product film in 0.137 mol/L HCl + 0.385 Na_2S solution.

Discussion

The micro-morphology of 2205 DSS surface in 0.137 mol/L HCl + 0.385 mmol/L Na_2S solution at 90°C looks like intergranular corrosion in some degree in the SEM images (Fig. 7h), showing many deep micro-holes and micro-cracks on the corroded surface, which indicates that the corrosion of 2205 DSS is significantly promoted by Na_2S addition. It is apparent that the corrosion mechanism is closely associated with the roles of Na_2S, which can easily hydrolyse to H_2S, HS^- and S^{2-} ions and then preferentially adsorb on the metal surface, competing [38, 39] with Cl^- in the hydrochloric acid solution. The proposed adsorption mechanism of Na_2S on the metal surface is shown in Fig. 12.

As shown in Fig. 12, H_{ad} represents the adsorption of H on the metal surface, H_{ab} represents the permeation of H into the metal, and H_T is H in the traps of the metal. Meanwhile, S^{2-} and HS^- ions have a poisoning effect on the recombination of H to H_2, which increases the quantity of H on the surface and promotes the internal diffusion of H [19]. When the H_T recombines to H_2, the pressure increases with the H_2 aggregating in the traps can cause brittleness and stress concentration. It is generally accepted that the main trapping sites of steels locate at grain boundaries [38] [39]. So that the initiation and propagation of corrosion are preferentially at grain boundaries.

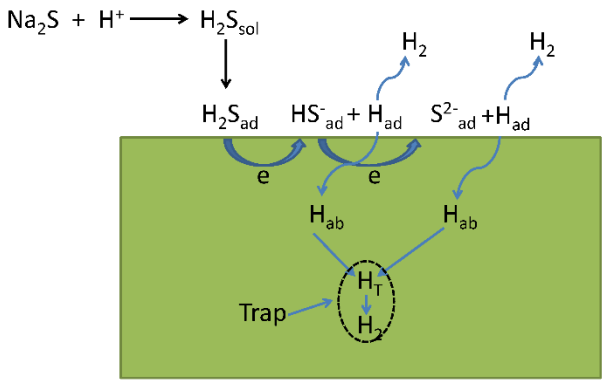

Fig.12 Adsorption mechanism of sulfide on metal surface.

Using 2205 DSS in this instance, Na_2S up to 3.846 mmol/L could not promote its corrosion distinctly in 0.1 mol/L HCl solutions at 90°C. However, in 0.137 mol/L HCl solution, the corrosion of 2205 DSS was extremely accelerated when the Na_2S concentration reached only 0.385 mmol/L. Additionally, 2205 DSS can remain stably passivated in HCl solution without Na_2S until the concentration increases to 0.584 mol/L. These results reveal that the combination effect of hydrochloric acid and sodium sulfide has two criteria: the first one is HCl concentration, and the second one is S^{2-} ion concentration. The possible corrosion mechanism of 2205 DSS in the investigated medium is presented in Fig. 13. As shown in Fig. 13a, 2205 DSS remains passivation in 0.1 mol/L HCl even though the passive film could be broken in a localized area by Cl^- attacking. However, the passive film of the attacked area could be repaired very quickly because of the excellent passivation ability of 2205 DSS. When the concentration of the HCl solution increases, the Cl^- attack becomes more severe, while the hydrogen reduction is enhanced. Thus, more defects would appear in the passive film, and its stability is clearly reduced in the 0.137 mol/L HCl solution, as shown in Fig. 13b,

supported by the sudden drop in pitting potential from 0.75 V to 0.4 V in the polarization curve measurement (Fig. 2a). Fig. 13c shows the corrosion mechanism of 2205 DSS in 0.1 mol/L HCl + Na_2S solution. The adsorption of S^{2-} and HS^- ions could accelerate the corrosion in some localized areas without passive film protection by promoting the cathodic hydrogen reduction reaction as indicated by the decrease in charge transfer resistance of the electrolyte/metal interface with increasing Na_2S concentration (R_2 of Table 1). On the other hand, most of the surface is under the good protection of the passive film, and the passive film even becomes more stable by adding Na_2S, as evidenced by the film resistance (R_1) being increased (Table 1). This phenomenon might be attributed to the competitive adsorption of S^{2-} and/or HS^- ions to prevent Cl^- attacking the passive film. However, as more defects exist in the passive film and surface in 0.137 mol/L HCl solutions, 2205 DSS cannot maintain stable passivation when N_2S reaches 0.385 mmol/L, and the degradation process is as described from Fig. 13d to Fig. 13e.

First, the hydrogen reduction and anodic dissolution are significantly accelerated at localized surficial defects. As shown in Fig. 13e, the destruction of the passivation can be ascribed to the interaction of H_2S, S^{2-} ion, HS^- ion, H^+ ion and Cl^- ion in defects when the concentrations of hydrochloric acid and Na_2S are concurrently high enough. It has been reported [40] that H_2S, S^{2-} and HS^- ions adsorbed on surfaces in defect sites of stainless steel could form FeS intermediate products. Then, the dissolution of FeS in hydrochloric acid produces H_2S. The regenerated H_2S again facilitates the corrosion of 2205 DSS. When the H_2S concentration and HCl concentration reach critical values, this process of autocatalysis could accelerate corrosion remarkably. On the other hand, sulfide can promote the diffusion of H into traps at grain boundaries. When H recombines to H_2 at grain boundaries along with acidic dissolution, severe intergranular corrosion occurs between the austenite and ferrite phases. With additional hydrogen generation and active dissolution sites expanding, the specimen can no longer maintain passivation, and active dissolution occurs shortly.

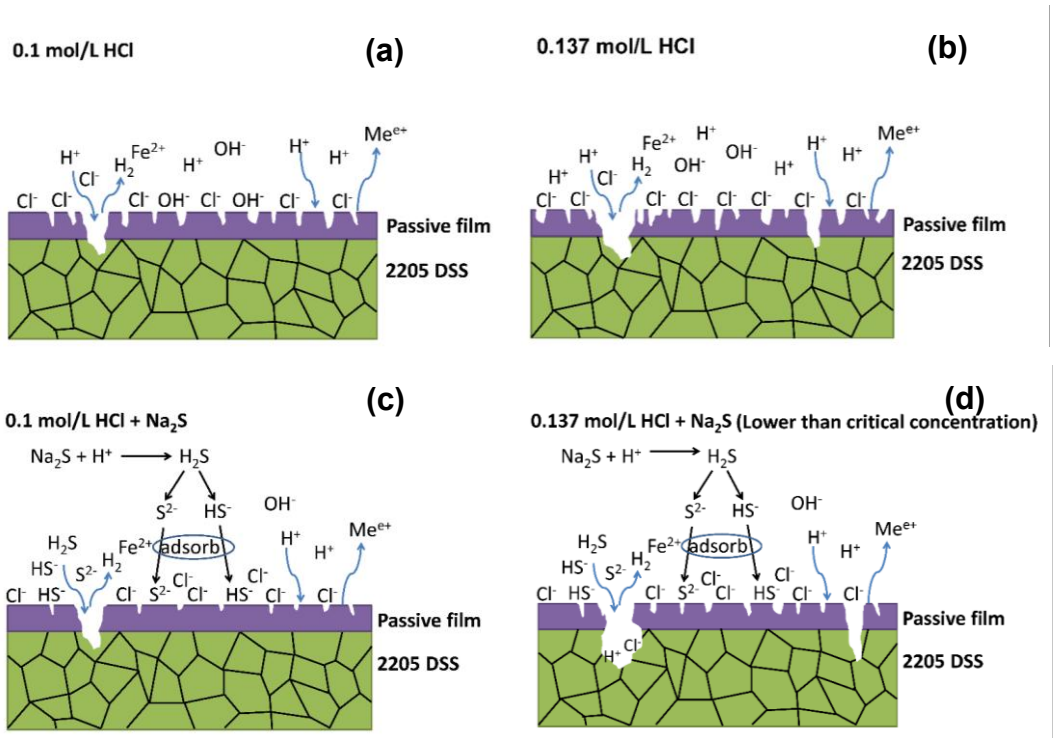

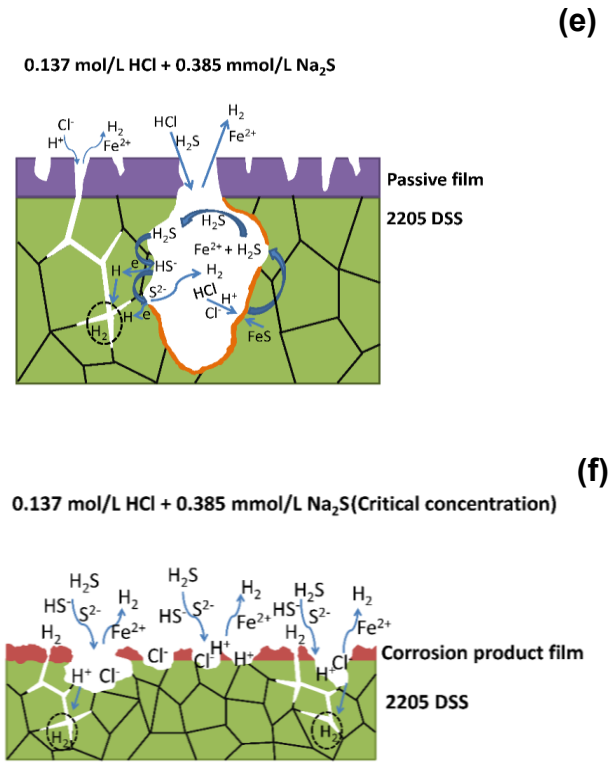

Fig. 14 Corrosion mechanism models of 2205 DSS: (a) 0.1 mol/L HCl, (b) 0.137 mol/L HCl, (c) 0.1 mol/L HCl + Na_2S (d) corrosion initiation in 0.137 mol/L HCl + Na_2S, (e) corrosion propagation 0.137 mol/L HCl + 0.385 mmol/L Na_2S, (f) inner of localized defect in 0.137 mol/L HCl + 0.385 mmol/L Na_2S.

Conclusions

The effects of sulfide on the corrosion behaviour of 2205 DSS in HCl solutions were investigated with mass loss tests, potentiodynamic polarization tests, EIS, SKP, SEM and XPS in this paper, and some important points are emphasized as below:

(1) 2205 DSS exhibited high corrosion resistance when the HCl concentration was lower than 0.274 mol/L. However, when 0.385 mmol/L Na_2S was added to HCl solutions at or above 0.137 mol/L, the corrosion resistance of 2205 DSS would be tremendously reduced, and active dissolution would occur.

(2) The SKP results showed that the surface potential distribution of 2205 DSS clearly changed after corrosion and that the anodic area enlarged. The micro-morphology revealed that 2205 DSS would undergo intergranular corrosion with deep mciro-holes and micro-cracks in HCl + Na_2S solution, while only general corrosion occurred in HCl solution without Na_2S.

(3) The passive film of 2205 DSS in dilute HCl with or without Na_2S is mainly composed of Cr(III) oxide-hydroxides with high chemical stability, which offer excellent protection for the 2205 DSS matrix. On contrast, the corrosion product film formed in active dissolution is mainly composed of metal (except Fe) oxides and/or hydroxides, sulfides, elemental sulfur and chlorides.

(4) S^{2-} and HS^- ions had high adsorption on 2205 DSS in HCl solutions. In 0.1 mol/L HCl solution, competitive adsorption between S^{2-}, HS^- and Cl^- ions would prevent the dissolution of the passive film. However, in 0.137 mol/L HCl + 0.385 mmol/L Na_2S solution, S^{2-} and HS^- ions mainly promoted the process of hydrogen evolution and surface depassivation. The combination effect of H^+, Cl^-, S^{2-} and HS^- ions would accelerate the corrosion remarkably when the concurrent concentrations of hydrochloric acid and Na_2S are sufficiently high.

References

1. B.S. Huang, W.F. Yin, D.H. Sang, Z.Y. Jiang, Appl. Surf. Sci. **259** (2012) 664-670.
2. Q. Cheng, B. Tao, L. Song, W. Zhang, X. Liu, W. Li, B. Hou, Q. Liu, Eval. Program Plann. **111** (2016) 61-71.
3. V. Moura, A.Y. Kina, S.S.M. Tavares, L.D. Lima, F.B. Mainier, J. Mater. Sci. **43** (2008) 536-540.
4. I.F. Vasconcelos, S.S.M. Tavares, F.E.U. Reis, H.F.G. Abreu, J. Mater. Sci. **44** (2009) 293-299.
5. L.S. Moiseeva, A.E. Aisin, Prot. Met. **43** (2007) 84-86.
6. C.C. Silva, J.P.S.E. Machado, A.V.C. Sobral-Santiago, H.B. de Sant'Ana, J.P. Farias, J. Pet. Sci. Eng. **59** (2007) 219-225.
7. A.P. Efremov, S.K. Kim, Prot. Met. **42** (2006) 194-200.
8. J. Mendoza-Canales, J. Marín-Cruz, J. Solid State Electrochem. **12** (2008) 1637-1644.
9. H. Tan, Y. Jiang, B. Deng, T. Sun, J. Xu, J. Li, Mater. Charact. **60** (2009) 1049-1054.
10. P.J. Antony, S. Chongdar, P. Kumar, R. Raman, Electrochim. Acta. 52 (2007) 3985-3994.
11. P. Kangas, G.C. Chai, Adv. Mater. Res. **794** (2013) 645-669.
12. S.-H. Jeon, S.-T. Kim, J.-S. Lee, I.-S. Lee, Y.-S. Park, Mater. Trans. **53** (2012) 1617-1626.
13. T. Wan, N. Xiao, H. Shen, X. Yong, Ultrason. - Sonochemistry. **33** (2016) 1-9.
14. D. Chaofang, L.U.O. Hong, X. Kui, S.U.N. Ting, L.I.U. Qian, L.I. Xiaogang, J. Wuhan Univ. Technol. Sci. Ed. **26** (2011) 641-647.
15. I. Lo, Y. Fu, C. Lin, W. Tsai, Corros. Sci. **48** (2006) 696-708.
16. Z.Y. Liu, C.F. Dong, X.G. Li, Q. Zhi, Y.F. Cheng, J. Mater. Sci. **44** (2009) 4228-4234.
17. R. Liu, J. Li, Z. Liu, C. Du, C. Dong, X. Li, Int. J. Mater. Res. **106** (2015) 608-613.
18. W. He, O.Ø. Knudsen, S. Diplas, Corros. Sci. **51** (2009) 2811-2819.
19. M.A. Veloz, I. Gonza, Electrochim. Acta. **48** (2002) 135-144.
20. J. Ding, L. Zhang, M. Lu, J. Wang, Z. Wen, W. Hao, Appl. Surf. Sci. **289** (2014) 33-41.
21. R.P. Case, H.E. Rincon, D.R. McIntyre, Corrosion. **68** (2012) 1-12.
22. P. Marcus, Electrochim. Acta. **43** (1998) 109-118.
23. P. Marcus, V. Maurice, H.H. Strehblow, Corros. Sci. **50** (2008) 2698-2704.
24. W. Fredriksson, D. Petrini, K. Edström, F. Björefors, L. Nyholm, Corros. Sci. **67** (2013) 268-280.
25. G.A. Zhang, Y. Zeng, X.P. Guo, F. Jiang, D.Y. Shi, Z.Y. Chen, Corros. Sci. **65** (2012) 37-47.
26. G. Herbsleb, R.K. Poepperling, Corrosion. **36** (1980) 611-618.
27. S.M. Bhola, R. Bhola, B. Mishra, D.L. Olson, J. Mater. Sci. Mater. Med. **22** (2011) 773-779.
28. S.M. Bhola, R. Bhola, B. Mishra, D.L. Olson, J. Mater. Sci. **45** (2010) 6179-6186.

29. Y.X. Qiao, Y.G. Zheng, W. Ke, P.C. Okafor, Corros. Sci. **51** (2009) 979-986.
30. H. Ma, X. Cheng, G. Li, S. Chen, Z. Quan, S. Zhao, L. Niu, Corros. Sci. **42** (2000) 1669-1683.
31. C. Azevedo, P.S. a. Bezerra, F. Esteves, C.J.B.M. Joia, O.R. Mattos, Electrochim. Acta. **44** (1999) 4431-4442.
32. H.Y. Ha, M.H. Jang, T.H. Lee, J. Moon, Understanding the relation between phase fraction and pitting corrosion resistance of UNS 32750 stainless steel, Elsevier B.V., 2015.
33. J. Kittel, V. Smanio, M. Fregonese, L. Garnier, X. Lefebvre, Corros. Sci. **52** (2010) 1386-1392.
34. H. Luo, C.F. Dong, K. Xiao, X.G. Li, Appl. Surf. Sci. **258** (2011) 631-639.
35. C.T. Liu, J.K. Wu, Corros. Sci. **49** (2007) 2198-2209.
36. A. Kawashima, K. Hashimoto, S. Shimodaira, Corrosion. **32** (1976) 321-331.
37. A. Bhattacharya, Æ.P.M. Singh, J. Fail. Anal. Prev. **7** (2007) 371-377.
38. G.P. Tiwari, A. Bose, J.K. Chakravartty, S.L. Wadekar, M.K. Totlani, R.N. Arya, R.K. Fotedar, Mater. Sci. Eng. A. **286** (2000) 269-281.
39. J. González, F. Gutiérrez-Solana, J.M. Varona, Metall. Mater. Trans. A. **27** (1996) 281-290.
40. F. Mancia, Corros. Sci. **27** (1987) 1225-1237.